

RESEARCH

Open Access



# The R2TP complex stabilises E7 to drive human papillomavirus-mediated pathogenesis in cellular models of cervical cancer

Mahaiwon Shadang<sup>1</sup>, Aruna Arumugam<sup>1,5</sup>, Dhiraj Kumar Singh<sup>1</sup>, Pankaj Keshari<sup>1</sup>, Sandeep Mathur<sup>2</sup>, Venkateswaran K. Iyer<sup>2</sup>, Seema Singhal<sup>3</sup>, Shyam S. Chauhan<sup>1</sup>, Qulsum Akhter<sup>4</sup> and Riyaz Ahmad Mir<sup>1\*</sup>

**Abstract** Human papillomaviruses (HPVs), particularly types 16 and 18, are major contributors to cervical cancer through the oncogenic activities of the E6 and E7 proteins. These viral proteins inactivate the tumour suppressors p53 and pRB, driving uncontrolled cellular proliferation. In this study, we investigated the interaction between the HPV E7 protein and the R2TP complex, a co-chaperone involved in essential cellular functions, including ribosome biogenesis, transcription, and macromolecular assembly. We identified PIH1D1, a core R2TP subunit, as an interacting partner of HPV16 and HPV18 E7 proteins. Mutagenesis and pull-down assays showed that phosphorylation of HPV E7 by casein kinase 2 (CK2) is critical for this interaction, as mutations of serine residues within the CK2 phospho-acceptor site on E7 disrupted the binding with PIH1D1. Furthermore, PIH1D1 facilitated the association of E7 with the retinoblastoma protein (pRB), forming a complex that likely promotes cancer cell proliferation. Immunohistochemical analysis of cervical cancer tissues revealed overexpression of PIH1D1, RUVBL1, and RPAP3—key components of the R2TP complex. Functional assays confirmed that PIH1D1 is crucial for cervical cancer cell growth and migration, as its silencing reduced E7 stability and impaired proliferation. Collectively, these findings highlight that PIH1D1, and by extension, the R2TP complex, is integral to the HPV-driven malignancy and suggest potential as therapeutic targets in HPV-related cancers.

**Importance** Despite being largely preventable through vaccination, cervical cancer is a significant concern for public health. Research is essential to understand the factors contributing to its high incidence and mortality and to devise effective prevention and treatment strategies. We investigated the functional role of PIH1D1, a core subunit of the R2TP complex, in the HPV-mediated cervical carcinogenesis. The interaction of the R2TP complex, HPV E7, and the tumour suppressor pRB proteins may be essential in driving malignant transformation.

**Keywords** Human papillomavirus, E7, Tumour virus, PRB, Cervical cancer, Chaperones, R2TP complex

\*Correspondence:

Riyaz Ahmad Mir

riyaz978@gmail.com; riyazmir@aiims.edu

<sup>1</sup>Department of Biochemistry, All India Institute of Medical Sciences, Delhi, India

<sup>2</sup>Department of Pathology, All India Institute of Medical Sciences, Delhi, India

<sup>3</sup>Department of Obstetrics and Gynaecology, All India Institute of Medical Sciences, Delhi, India

<sup>4</sup>Department of Biochemistry, Government Degree College Pulwama, Jammu, Kashmir, India

<sup>5</sup>Present address: Institute of Chemistry and Biochemistry, Laboratory of Structural Biochemistry, Freie Universität Berlin, Takustr. 6, D-14195 Berlin, Germany



© The Author(s) 2026. **Open Access** This article is licensed under a Creative Commons Attribution-NonCommercial-NoDerivatives 4.0 International License, which permits any non-commercial use, sharing, distribution and reproduction in any medium or format, as long as you give appropriate credit to the original author(s) and the source, provide a link to the Creative Commons licence, and indicate if you modified the licensed material. You do not have permission under this licence to share adapted material derived from this article or parts of it. The images or other third party material in this article are included in the article's Creative Commons licence, unless indicated otherwise in a credit line to the material. If material is not included in the article's Creative Commons licence and your intended use is not permitted by statutory regulation or exceeds the permitted use, you will need to obtain permission directly from the copyright holder. To view a copy of this licence, visit <http://creativecommons.org/licenses/by-nc-nd/4.0/>.

## Introduction

Human papillomaviruses (HPVs) rank second in the list of infectious agents that cause cancer. HPVs are associated with cancers of the vulva, vagina, cervix, mouth/throat, penis, anus, and head and neck [1]. Globally, cervical cancer is the fourth most common cancer in women and in India, it ranks second [2]. Infections by HPVs typically occur through micro-abrasions in the tissue and infect basal cells of the epithelium of vertebrates [3]. Of approximately 17 high-risk HPV types, HPV types 16 and 18 account for 78% of cervical cancer cases, while types 31, 33, 45, 52, and 58 account for an additional 18% [4]. The oncoproteins encoded by high-risk HPVs, E6 and E7, interact with a myriad of host proteins to drive tumorigenesis [3, 5]. Abrogation of E6 and E7 expression resulted in growth arrest followed by apoptosis or senescence, making E6 and E7 potential targets for therapeutic intervention in HPV-mediated cancers [6, 7]. The best-known cellular targets of HPV are the tumour suppressors, p53 and pRB [8–11]. The binding of E7 to pRB induces the degradation and functional inactivation of pRB, releasing the transcription factor E2F1 from the E2F-pRB complex, allowing the transcriptional activation of E2F1-responsive promoters and the transition of cells from G0/G1 to S-phase [8, 12]. E6 interacts with E6-associated protein (E6AP), an E3 ubiquitin ligase, and targets the p53 protein for degradation [8, 9]. Although E6 and E7 have been extensively studied, there are still significant gaps in our understanding of how these proteins interact with and inactivate the tumour suppressor proteins pRB and p53, ultimately leading to malignancy.

The R2TP complex is an evolutionarily conserved cochaperone of Hsp90 [13, 14]. In mammals, the complex consists of RUVBL1 (RuvB-like 1), RUVBL2 (RuvB-like 2), PIH1D1 (PIH1 domain-containing protein 1), and RPAP3 (RNA polymerase II-associated protein 3) and also associates with prefoldin and prefoldin-like proteins. This hetero multimeric structure is called the PAQosome, Particle for Arrangement of Quaternary Structure [15]. The complex is involved in many cellular pathways, including small nucleolar ribonucleoprotein particles (snoRNPs) biogenesis and assembly, telomerase complex assembly, RNA polymerase II assembly, phosphatidylinositol 3-kinase-related protein kinases (PIKKs) signalling and apoptosis, where the R2TP subunits interact with various subunits of these multiprotein complexes [14–16]. The molecular biology underlying the recognition of diverse substrates by the R2TP/PAQosome-Hsp90 complex and the context-dependent cellular consequences of these interactions are still poorly understood. Clarifying the cellular functions of the R2TP/PAQosome will require the identification of additional clients and adaptors. However, the involvement of the R2TP complex in numerous cellular functions suggests that

its dysregulation or perturbation could have detrimental effects on the cell. Several studies demonstrate that the R2TP could play essential roles in pathogenic cellular proliferation, besides assembling and stabilising macromolecular complexes [17–20].

A mechanism through which the R2TP complex selectively recruits its clientele is via PIH1D1. PIH1D1 recognises substrates/adaptors phosphorylated by casein kinase 2 and bridges client proteins to the R2TP-Hsp90 complex [21, 22]. The HPV E7 protein has a phospho-acceptor site for CK2 within the N-terminal in the CR2 domain, downstream of the LxCxE motif where pRB binds [23]. The serine residues are S31 and S32 in HPV 16 and S32 and S34 in HPV 18, respectively [24, 25]. This motif is conserved among the different HPV types and in the SV40T and AdE1A proteins from Simian Virus 40 and Adenovirus, respectively [26]. Therefore, the CK2 phospho-acceptor site could be fundamental for their biology [27, 28]. It has been suggested that these proteins might recruit chaperones to disrupt the function of pocket protein pRB/E2F complexes [29–32]. Based on this rationale, we show that PIH1D1 interacts with the E7 proteins of high-risk HPV types 16 and 18 and the pRB protein. The mutation of serine residues within the CK2 phospho-acceptor site of HPV16 E7 to alanine abolishes the phosphorylation by CK2, thereby eliminating the interaction of PIH1D1 with E7. In cervical cancer cells, HPV E7 likely recruits PIH1D1 to the pRB-E7 complex to drive proliferation. We also observed decreased levels of E7 when PIH1D1 was depleted in cells. Furthermore, PIH1D1 and RPAP3 are overexpressed in cervical cancer tissues.

## Materials and methods

### Cell culture

Cell lines HEK293, C33A, HeLa, and CaSki were obtained from the National Centre for Cell Science, Pune, India, and T98G cells were purchased from the American Type Culture Collection, USA. HEK293, C33A, MCF7, T98G and HeLa cells were grown in Dulbecco's Modified Eagle Medium (HiMedia, Cat. AL007A) and CaSki cells were grown in RPMI (Gibco, Cat. 164011875093) supplemented with 10% Fetal Bovine Serum (Gibco, Cat. 10270106) and Antibiotic-Antimycotic 100X (Gibco, Cat. 15240096). The cells were grown in an atmosphere of 5% CO<sub>2</sub> at 37 °C and were sub-cultured by trypsinisation with Trypsin - EDTA Solution 1X (HiMedia, Cat. TCL014). The MCF7 cell line was from Dr Chauhan's lab, AIIMS, New Delhi.

### Plasmids

pCMV6-AC-GFP-PIH1D1 (Cat. RG200158) was purchased from Origene, USA. PGEX-2T E7 (#13634), MSCV-C 18E7 (#37886), and pCMV HA hRB-wt

(#58905) were purchased from Addgene. pcDNA3.1+ and hnRNP constructs were from Dr Chauhan's lab, AIIMS, New Delhi.

### Cloning of PIH1D1

In-Fusion® HD Cloning Kit (Takara Bio USA, Inc., Cat. 102518) was used for subcloning PIH1D1 from vector pCMV6-AC-GFP-PIH1D1 (Origene, USA) to the recipient vector PGEX-2T. PCR primers for PIH1D1 (Table 1) were designed using the In-Fusion Cloning Primer Design Tool (<https://takara.teselagen.com/#/DesignPage>). Linearised PGEX-2T vector was generated using restriction enzymes, BamH1 and EcoR1 (Thermo Scientific™ FastDigest EcoR1, FD0275 and BamH1, FD0054). Successful ligations were screened by restriction digestion and colony PCR. Recombinant GST-PIH1D1 proteins were purified from BL21(DE3) cells using the protocol described.

### Cloning of E7

HPV 18E7 was subcloned from MSCV-C 18E7 to PGEX-2T. HPV 16E7 coding sequences were subcloned from the PGEX-2T constructs to pcDNA3.1+ vectors to express E7 proteins (wild-type and mutated) in mammalian systems. (Primers listed in Table 1) Restriction digest for PCR products and the recipient vector was performed with BamH1 and EcoR1. The digested fragments were ligated with T4 DNA Ligase (5 U/μL) (Thermo Scientific™, Cat. EL0011) and transformed into competent DH5α cells. pcDNA 3.1+ - E7 wildtype (1) and mutants (3) plasmids were then transfected into the HEK293 cell line to express E7 in vivo.

### Site-directed mutagenesis

To generate constructs harbouring mutations on E7, SDM was performed using the Phusion Site-Directed Mutagenesis Kit (Thermo Scientific™, Cat. F541) with PGEX-2T 16E7 as the template. The PCR reactions were optimised according to the manufacturer's instructions and primers listed in Table 1. Plasmids were isolated

from the resulting colonies using the QIAprep Spin Miniprep Kit (Cat. 27104) and screened for the desired modifications by Sanger sequencing.

### Expression and purification of GST fusion proteins

A single colony was resuspended in 10 ml of Luria Bertani (LB) medium (HiMedia, Cat. M1245) supplemented with 100 μg/ml ampicillin (SRL, Cat. 61314) and grown overnight at 37 °C with shaking at 200 rpm. The following day, 10 ml of the overnight culture was added to 90 ml of LB medium supplemented with 100 μg/ml ampicillin. This culture was grown at 37 °C with shaking at 200 rpm until the OD600 reached 0.5–0.7. Then, the culture was induced with isopropyl β-D-1-thiogalactopyranoside (Promega, Cat. V3953) (final concentration 1 mM) and grown for an additional 3 h at 37 °C at 200 rpm. The bacteria were harvested by centrifugation at 4000 × g for 20 min at 4 °C. The supernatant was discarded, and the pellet was stored at –80 °C until ready to proceed with the purification.

The cell pellets were subsequently resuspended in cold 5 mL of lysis buffer (10 mM Tris-HCl, 0.1 mM EDTA, and 150 mM NaCl). The cells were sonicated after the addition of 10% sarkosyl (SRL, India, Cat. 74090), and the insoluble material was removed by centrifugation at 4000 rpm at 4 °C for 20 min. The clarified lysate was transferred to a 15 ml Falcon tube supplemented with 10% Triton X-100 (BR Biochem Life Sciences, Cat. BC0198). For a 100 ml culture, 35 μl of glutathione resin (GBioScience, USA, Cat. 786–280) was added to the tube and incubated overnight in a rotating motion at 4 °C. Before incubation, the glutathione resins were washed with 5 mL of 1X PBS three times by centrifugation at 4 °C at 3000 rpm for 3 min. The following day, the beads were recovered first by centrifugation at 4 °C at 3000 rpm. The beads were subsequently washed with 5 ml of 1X PBS three times by centrifugation at 4 °C and 3000 rpm. The eluted beads were mixed with Laemmli buffer for denaturing at 95 °C for 5 min and subjected to SDS-PAGE. Each step of the purification process was analysed by SDS-PAGE and stained with Coomassie Brilliant Blue (SRL, India, Cat. 93473). The eluted beads were quantified by SDS-PAGE by loading varying concentrations of BSA protein (NEB, Cat. B9200S).

### GST pull-down assay

Purified GST fusion proteins or GST were incubated overnight with 1–2 mg/ml crude cell lysates. The following day, the reaction was centrifuged at 4 °C at 3000 rpm for 3 min to sediment the beads. The eluted proteins were analysed by SDS-PAGE followed by Western blotting.

**Table 1** List of primers for the cloning of HPV 16 E7 and PIH1D1

HPV 16E7	Forward	CGGGATCCATGCATGGAGATACACCT
	Reverse	CGGAATTCCTATGTTTCTGAGAACA
HPV 18E7	Forward	CGGGATCCATGCATGGACCTAAG
	Reverse	CGGAATTCCTACTGCTGCTGCTG
PIH1D1	Forward	GGTTCCGCGTGATCCATGGCGAACCCGAAGCTG
	Reverse	CAGTCACGATGAATTCTCAAGAAGGCACCCGCCAG
16E7 S31A	Forward	TTAATGACGCCTCAGAGGAGGAG
	Reverse	CTCCTCTCTGAGGCGTCATTAA
16E7 S32A	Forward	TTAATGACAGCGCAGAGGAGGAG
	Reverse	CTCCTCTCTGCGCTGTCATTAA
16E7 S31/ S32A	Forward	TTAATGACGCCGAGAGGAGGAG
	Reverse	CTCCTCTCTGCGCTGTCATTAA

### Co-immunoprecipitation

1–2 mg/ml crude cell lysates were incubated overnight with 1–2 µg antibodies or 1 µg of IgG Isotype (Invitrogen, Cat. 31154) at 4 °C. The following day, the antigen-antibody complex was immunoprecipitated with Protein A/G PLUS-Agarose (Santacruz, Cat. sc-2003) for 4 h at 4 °C with gentle agitation.

### In vitro kinase assay

Purified GST-E7 fusion proteins were phosphorylated by Casein kinase 2 (New England Biolabs, Cat. P6010S) in the presence of 1X NEBuffer (50mM Tris-HCl, 10mM MgCl<sub>2</sub>, 0.1 mM EDTA, 2mM DTT, 0.01% Brij 35) and 200µM ATP (New England Biolabs, Cat. P0756S) for 30 min at 30 °C. To stop the reaction, Laemmli buffer was added.

### Transfection

1 × 10<sup>5</sup> cells were seeded in 6-well cell culture plates 24 h before the experiment to achieve 70% confluency. Then cells were serum starved for 4 to 16 h before the addition of plasmid DNA or siRNA. Lipofectamine™ 3000 Transfection reagent (Invitrogen™, Cat. L3000001) and Lipofectamine RNAiMax reagent (Cat. 13778030) were used according to the manufacturer's instructions. Analyses of protein levels were carried out 48 h after transfection. An empty vector or AllStars Negative Control siRNA (5 nmol) (Qiagen, Cat. 1027280) was used as a control. siRNAs used in this study were NOP17 siRNA(h) (Santa Cruz, sc-97385) and HPV16 E7 siRNA (hvp) (Santa Cruz, sc-270423).

### Western blotting

After electrophoresis with SDS-PAGE, the separated proteins were transferred onto a PVDF membrane (0.22 or 0.45-µm pore size; Merck Millipore) at 300 MA for 1 h in ice-cold 20% (vol/vol) methanol transfer buffer. After transfer, the membrane was stained with Ponceau S (SRL, Cat. 38610) and washed with distilled water using a shaker. The membrane was blocked with 5% non-fat milk powder (HiMedia, Cat. GRM1254) or 3% Bovine Serum Albumin/BSA (SRL, Cat. 85171) in 1X TBS-T buffer for 1 h at room temperature. The membrane was incubated with primary antibodies overnight at 4 °C and the following day, with secondary antibodies for 1 h at room temperature. All the antibodies were diluted in 1% blocking buffer. Proteins were visualised using Pierce™ ECL Western Blotting Substrate (Thermo Scientific™, Cat. 32109) or femtoLUCENT™ PLUS-HRP (G-Biosciences, Cat. 786–081). When probing for multiple targets, stripping and re-probing the same membrane is achieved by several washes with a mild stripping buffer (Glycine-SDS-Tween 20, pH 2.2) and 1X TBS-T buffer.

### MTT assay

Cells were seeded at a density of 1 × 10<sup>6</sup> cells/ml into a 96-well microplate to a volume of 100 µL/well, in triplicate. Wells (with medium alone) were kept as blanks (controls) for the absorbance readings. The cells were incubated at 37 °C with 5% CO<sub>2</sub> overnight. 24–96 h after seeding, 10µL of the MTT reagent (Invitrogen™, Cat. M6494) (12mM) was added to each well and incubated for 3 h at 37 °C. 100 µL of DMSO was added to each well for 10 min at 37 °C in the dark. Absorbance was read at 570 nm. The calculation for relative % viability is given below:

$$\text{Relative \% viability} = [\text{OD}(\text{siPIH1D1}, t_n) / \text{OD}(\text{siScramble}, t_n)] * 100.$$

### Wound healing assay

1 × 10<sup>4</sup> cells were seeded on a 12-well plate overnight and treated with siRNA or scramble siRNA. 48 h later, the confluent monolayer was gently scratched across the centre of the well using a sterile 200 µl pipette tip. After scratching, the well was gently washed once with 1X PBS to remove any detached or dead cells. The well was then replenished with the appropriate media. Images were captured at 10X magnification in a bright-field microscope at different time points. The wound closure % was calculated on the ImageJ software [57].

### Cycloheximide treatment

siRNA knockdown of PIH1D1 and siScramble (control) was performed in HeLa cells, followed by incubation for 72 h. Before harvesting, cells were further treated with cycloheximide (100 µg/ml) (Sigma-Aldrich, Cat. C4859) for different time periods. The cells were harvested at each time point and analysed by Western blotting.

### Immunofluorescence staining

Cells were seeded at a density of 1 × 10<sup>4</sup> cells/well on clean and coated coverslips (Gibco, Cat. A3890401) placed in 6-well plates at 37 °C and 5% CO<sub>2</sub>. Twenty-four hours after cell seeding, the cells were fixed with 4% paraformaldehyde (HiMedia, Cat. TCL119) for 15 min. The fixed cells were permeabilised with 0.1% Triton X-100-PBS for 15 min at room temperature. Blocking was performed with 1% BSA (protease-free) for 30 min at room temperature with gentle shaking. After three washes, the cells were incubated with primary antibodies against RPAP3, PIH1D1, and HPV 16 E7 at a 1:200 dilution at 4 °C overnight. The following day, cells were then incubated with fluorescent dye-labelled secondary antibodies for 2 h in the dark. Nuclei were counterstained with DAPI solution (1 mg/mL) (Thermo Scientific™, Cat. 62248) for 5 min. The labelled cells on coverslips were mounted on a clean glass slide with 50% glycerol in 1X

PBS. Images were acquired with a confocal microscope and software and analysed with ImageJ.

#### Proximity ligation assay

Duolink® In Situ Orange Starter Kit Mouse/Rabbit (Sigma-Aldrich, Cat. DUO92102) was used, as per the manufacturer's instructions, for the Proximity Ligation Assay. A pair of oligonucleotide-labelled antibodies (PLA probes) generates an amplified signal only when the probes are in proximity (<40 nm). Cells were seeded at a density of  $1 \times 10^4$  cells/well on clean and coated coverslips (Gibco, Cat. A3890401) placed in 6-well plates at 37 °C and 5% CO<sub>2</sub>. Twenty-four hours after cell seeding, the cells were fixed with 4% paraformaldehyde (HiMedia, Cat. TCL119) for 15 min. The fixed cells were permeabilised with 0.1% Triton X-100-PBS for 15 min at room temperature. The cells were incubated with primary antibodies against RPAP3, PIH1D1, RB and HPV 16 E7 at a 1:25 dilution at 4°C overnight. Images were acquired with a confocal microscope and software, and analysed with Fiji. Cells were treated with CX-4945 (MCE, Cat. HY-50855) for 24 h before fixing. Images were captured with a Laser scanning confocal microscope (LSM 980; Carl Zeiss, Germany). All the fluorescence images were captured under the same settings for every experimental set. Quantification of PLA signals (orange puncta) was performed on discrete regions of a single optical slice. For quantification, twenty cells were counted, and regions of interest (ROIs) were drawn for each cell. Data was represented as the number of PLA puncta per cell.

#### Immunohistochemistry

Ethical clearance was obtained from the institutional review board before the start of the study (IECPG-152/23.04.2020). As there is no prior study on our objective, we enrolled the number of cases listed. The formalin-fixed, paraffin-embedded tissue blocks were obtained from the archives of the Department of Pathology, AIIMS, Delhi. Briefly, 3–5 µm tissue sections on poly-L-lysine-coated slides were deparaffinised in xylene and rehydrated in a graded series of alcohol. Microwave-mediated antigen retrieval was performed using either Citrate or Tris-EDTA buffers. UltraVision Quanto Detection System HRP DAB (Thermo Scientific TL-060-QHD) was used according to the manufacturer's instructions. Each batch was run with an appropriate positive and negative control. Stained slides were scored for their intensity in a blinded manner by a pathologist. They were graded as score 1+, 2+, and 3+ based on the following criteria: (i) Score 1+: 10–30% positive cells, (ii) Score 2+: 30–50% positive cells, and (iii) Score 3+: >50% positive cells (i.e. 0 = no staining, 1 = weak, 2 = moderate and 3 = strong staining).

#### Antibodies

For Western blotting, the following primary antibodies were used: beta-actin (C4) (Santa Cruz, Cat. sc-47778) and p-Ser/Phosphoserine (4A3) (Santacruz, Cat. sc-81516). For co-immunoprecipitations, the following antibodies were used: HPV16 E7 (ED17) (Santa Cruz, Cat. sc-6981), HPV18 E7 (F-7) (Santa Cruz, Cat. sc-365035) and NOP17/PIH1D1 (18Y9) (Santa Cruz, Cat. sc-101000), Rabbit IgG Isotype Control (Invitrogen, Cat. 02–6102) and TELO2 (protein tech, Cat. 15975-1-AP).

For the immunofluorescence staining, the following antibodies were used: PIH1D1 (18Y9) (Santa Cruz, Cat. sc-101000), HPV16 E7 (ED17) (Santa Cruz, Cat. sc-6981), and RPAP3 (Thermo Fisher, Cat. PA5-58334), goat anti-rabbit IgG conjugated with TRITC (GeNei, Cat. 1120680011730), and goat anti-mouse IgG conjugated to FITC (GeNei, Cat. 1120380011730). Secondary antibodies were HRP-conjugated Goat anti-rabbit IgG (H+L) (Elabscience, Cat. E-AB-1003) and HRP-conjugated Goat anti-mouse IgG (H+L) (ABclonal, Cat. AS003).

For the proximity ligation assay, the following antibodies were used: PIH1D1 (Thermo Fisher, Cat. PA5-61482), RPAP3 (Thermo Fisher, Cat. PA5-58334), Human Retinoblastoma Protein [Clone G3-245 (RUO), BD Pharmingen™, Cat. 554136], and HPV16 E7 (ED17) (Santa Cruz, Cat. sc-6981).

For immunohistochemistry, the following antibodies were used: RUVBL1 (Proteintech, Cat. 10210-2-AP), PIH1D1 (Thermo Fisher, Cat. PA5-61482), and RPAP3 (Thermo Fisher, Cat. PA5-58334).

#### Statistical analysis

All data analyses were done with GraphPad Prism 8. The Student's t-test was applied for parametric data, and the Mann-Whitney test was used for non-parametric data. Statistical significance was defined at a p-value less than 0.05 ( $p < 0.05$ ). P values are defined as follows: \* $p < 0.05$ , \*\* $p < 0.01$ , \*\*\* $p < 0.001$ , \*\*\*\* $p < 0.0001$ , “ns” represents a non-significant P value above 0.05.

#### Results

##### PIH1D1 interacts with both HPV18 and 16 E7 protein in cells

Proteins such as TELO2, ECD, and MRE11, which interact with PIH1D1, contain a consensus motif DSDD/EE phosphorylated by CK2 [21]. (Fig. 1A) The HPV E7 oncoproteins have this CK2 phospho-acceptor site in the CR2 domain, downstream of the LxCxE motif, where the retinoblastoma gene product pRB binds. (Fig. 1B) As previously reported [23, 27], the site remains conserved in HPVs. (Fig. 1C) To determine whether E7 is a genuine interacting partner of the R2TP complex, we performed co-immunoprecipitation assays (co-IPs) with cervical cancer cells. Lysates from cervical cancer cell line HeLa

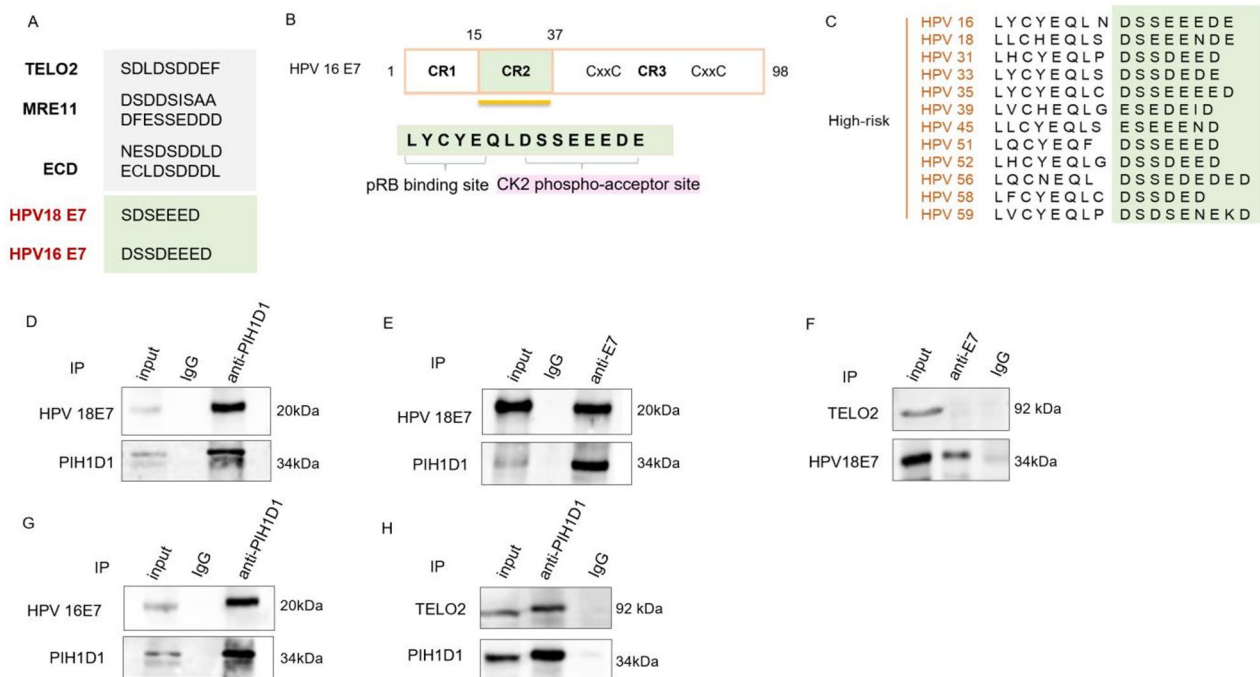


**Fig. 1** PIH1D1 interacts with HPV16 and HPV18 E7 proteins in CaSki and HeLa cells, respectively. **A**. The phospho-acceptor site on adaptors TELO2, MRE11, and ECD facilitates their interaction with PIH1D1. **B**. Schematic representation of HPV16 E7. Serine residues S31 and S32 are on the consensus phospho-acceptor site of CK2 in the CR2 domain of the protein. **C**. The phospho-acceptor site of CK2 is conserved in E7 proteins of HPV high-risk types, as previously reported. Sequences were obtained from and aligned using Papillomavirus Episteme (PaVE) (<https://pave.niaid.nih.gov>). **D**. 1 mg of HeLa cell lysate (HPV 18+) was subjected to co-immunoprecipitation with 1  $\mu$ g anti-PIH1D1 antibody, followed by western blotting with HPV 18E7 and PIH1D1 antibodies, and incubation of cell lysates with IgG Isotype control antibody serves as a negative control for the experiments. The input was 10% of the total protein used in the pull-down. **E**. Reverse co-immunoprecipitation of HeLa cell lysates with an anti-18E7 antibody, followed by western blotting with HPV 18E7 and PIH1D1 antibodies. **F**. 1 mg of HeLa cell lysate (HPV 18+) was subjected to co-immunoprecipitation with 1  $\mu$ g anti-E7 antibody, followed by western blotting with TELO2 and HPV 18E7 antibodies, and incubation of cell lysates with IgG Isotype control antibody serves as a negative control for the experiments. The input was 10% of the total protein used in the pull-down. **G**. 1 mg of CaSki Cell lysate (HPV 16+) was subjected to co-immunoprecipitation with 1  $\mu$ g anti-PIH1D1 antibody, followed by western blotting with HPV 16E7 and PIH1D1 antibodies. **H**. 1 mg of CaSki cell lysate (HPV 16+) was subjected to co-immunoprecipitation with 1  $\mu$ g anti-PIH1D1 antibody, followed by western blotting with TELO2 and PIH1D1 antibodies, and incubation of cell lysates with IgG Isotype control antibody serves as a negative control for the experiments. The input was 10% of the total protein used in the pull-down

(HPV18+) were subjected to co-immunoprecipitation with an anti-PIH1D1 antibody. As shown in Fig. 1D, PIH1D1 was able to co-immunoprecipitate HPV18 E7. Next, we performed reverse co-IP using an anti-18E7 antibody. As expected, HPV 18E7 co-immunoprecipitated PIH1D1 (Fig. 1E) while it did not co-immunoprecipitate TELO2 (Fig. 1F), indicating a specific interaction between E7 and PIH1D1. Similarly, co-immunoprecipitation was performed with lysates from the cervical cancer cell line CaSki (HPV16+) using an anti-PIH1D1 antibody, confirming that PIH1D1 interacts with HPV16 E7. (Fig. 1G) Since PIH1D1 interacts with TELO2 in a phosphorylation-dependent manner, the interaction served as a positive control. (Fig. 1H) Thus, we showed that PIH1D1 interacts with HPV16 and HPV18 E7 proteins in CaSki and HeLa cells, respectively.

#### PIH1D1 interacts with both HPV18 and 16 E7 proteins in vitro

To further validate the interaction observed between endogenous PIH1D1 and E7 proteins of HPV16 and 18, we performed a GST pull-down assay with recombinant GST-tagged E7 proteins. GST-tagged HPV 16E7 and 18E7 proteins were purified (Fig. 2A) and subsequently phosphorylated in vitro using enzyme CK2. The lysates from T98G cells were incubated with unphosphorylated and phosphorylated recombinant GST-tagged HPV 16E7 and 18E7 proteins. The final eluate was analysed by western blotting with antibodies against PIH1D1 and pRB. (Note: RB and pRB refer to the same retinoblastoma protein; the anti-RB antibody detects hypo- and hyperphosphorylated forms, therefore, the notation *pRB* is used throughout the text to denote the phosphoprotein.) Consistent with our observations of endogenous interactions, we found recombinant phosphorylated E7 proteins interacted with PIH1D1. (Fig. 2B, C) Notably, the phosphorylated E7 proteins exhibited a substantially stronger

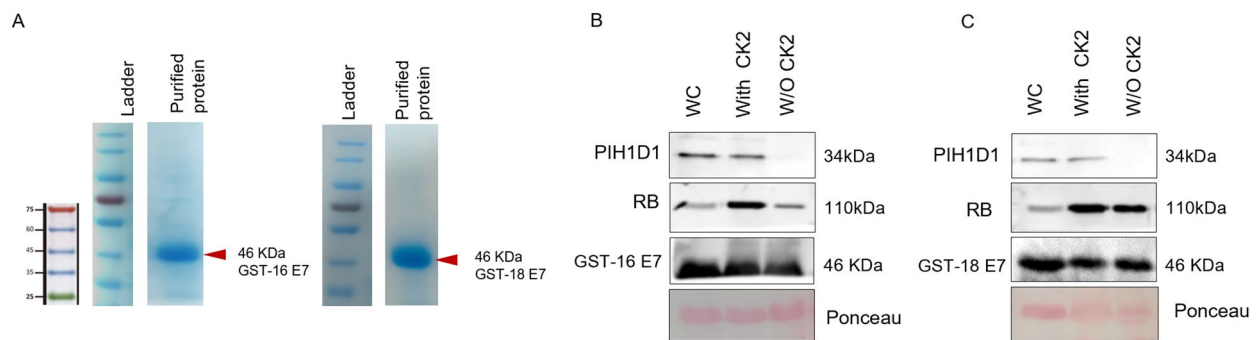


**Fig. 2** In vitro binding assay of recombinant purified GST-tagged HPV16 and 18 E7 proteins with PIH1D1. **A.** Recombinant GST-tagged E7 proteins were expressed in *E. coli*. Coomassie staining shows the purified GST-tagged HPV16 E7 and GST-tagged HPV18 E7 (~46 kDa) and molecular weight markers (left) (G-Biosciences, 786–419, PAGEmark Tricolour PLUS). **B.** Purified GST-HPV16 E7 (200 ng) was in vitro phosphorylated by CK2. Equal amounts of phosphorylated and unphosphorylated GST-16E7 proteins were incubated with 1 mg of T98G cell lysates for 4 h, followed by a GST pull-down assay and western blot analysis using PIH1D1, pRB, and E7 antibodies. **C.** Purified GST-HPV18 E7 (200 ng) was in vitro phosphorylated by CK2. Equal amounts of phosphorylated and unphosphorylated GST-18E7 proteins were incubated with 1 mg of T98G cell lysates for 4 h, followed by a GST pull-down assay and western blot analysis using PIH1D1 and pRB antibodies

interaction with PIH1D1 than the unphosphorylated proteins, and as expected, pRB was pulled down by both HPV16 E7 and HPV18 E7. Unlike HPV16 E7, the interaction of HPV18 E7 with pRB remains largely unaffected following CK2-mediated phosphorylation, indicating a possible type-specific modulation of E7–pRB binding by CK2. To rule out nonspecific binding or GST-mediated interactions, GST-hnRNPD was used as a control, with no interaction observed. (Suppl Fig. 1)

#### HPV E7 proteins colocalise with PIH1D1-RPAP3 of the R2TP complex

Having shown that E7 interacts with PIH1D1 in vitro and in vivo, we aimed to determine the site of the interaction in a relevant cellular context. Accordingly, we labelled CaSki cells with antibodies against PIH1D1, RPAP3, and E7. The PIH1D1 and 16 E7 antibodies in this experiment were generated in mice, whereas the RPAP3 antibody was produced in rabbits. Consequently, we labelled with the combinations: PIH1D1 + RPAP3 and E7 + RPAP3. The colocalization analysis was performed using the ImageJ software and an open-source plugin, JACoP. Notably, in CaSki cells, both PIH1D1 and RPAP3 were observed in the nucleus and cytoplasm, while HPV16 E7 was observed predominantly in the nucleus. (Fig. 3) PIH1D1 and RPAP3 were colocalised in the nucleus and cytoplasm (Manders' coefficients,  $M1=0.737$  and  $M2=0.937$ ). RPAP3 and HPV 16 E7 were predominantly colocalised in the nucleus (Manders' coefficients,  $M1=0.97$  and  $M2=0.656$ ).

The endogenous protein-protein interactions were validated in HPV-positive SiHa and CaSki cells using the proximity ligation assay. (Fig. 4A) C33A cells, which are HPV-negative cervical epithelial cells, were included as a control. PIH1D1-RPAP3 and HPV 16 E7

interactions were observed in the nucleus and the cytoplasm. We quantified the puncta in the cytosol and nuclei of SiHa and CaSki cells, respectively and observed the PIH1D1 + E7 interaction to be localised predominantly in the cytoplasm rather than the nucleus. (Fig. 4C) Treatment of these cells with CX4945, an inhibitor of CK2, disrupted the interaction of the R2TP complex with E7. (Fig. 4B)

#### The CK2 phosphorylation site of E7 is indispensable for interaction with PIH1D1

Both HPV 16E7 and 18E7 are phosphorylated by CK2. To determine whether the interaction between E7 and PIH1D1 is indeed dependent on the phosphorylation of E7 by CK2, we generated single and double amino acid substitutions within the CK2 phospho-acceptor site of HPV 16 E7 using site-directed mutagenesis. We generated three mutants in which serine residues 31 and 32 were changed to alanine: S31A (single), S32A (single), and S31/32A (double mutant, DM). (Fig. 5A) Then, we performed a GST pull-down assay. Purified GST-16 E7 wildtype and mutant proteins were first subjected to an in vitro kinase assay using CK2. Both phosphorylated and unphosphorylated E7 proteins were then incubated with HEK293 cell lysates, followed by SDS-PAGE and immunoblotting with anti-PIH1D1 and anti-phosphoserine antibodies. As expected, unphosphorylated GST-E7 proteins did not pull down PIH1D1. (Fig. 5B) However, phosphorylated proteins (GST-E7 WT, S31A, and S32A) successfully pulled down PIH1D1 from HEK293 cell lysates (Fig. 5B), and phosphorylation was confirmed by an anti-phosphoserine antibody. The double mutant of 16 E7 (DM), with both serines mutated to alanine, was unable to pull down PIH1D1 from cell lysates. The interaction between E7 and PIH1D1 was eliminated when

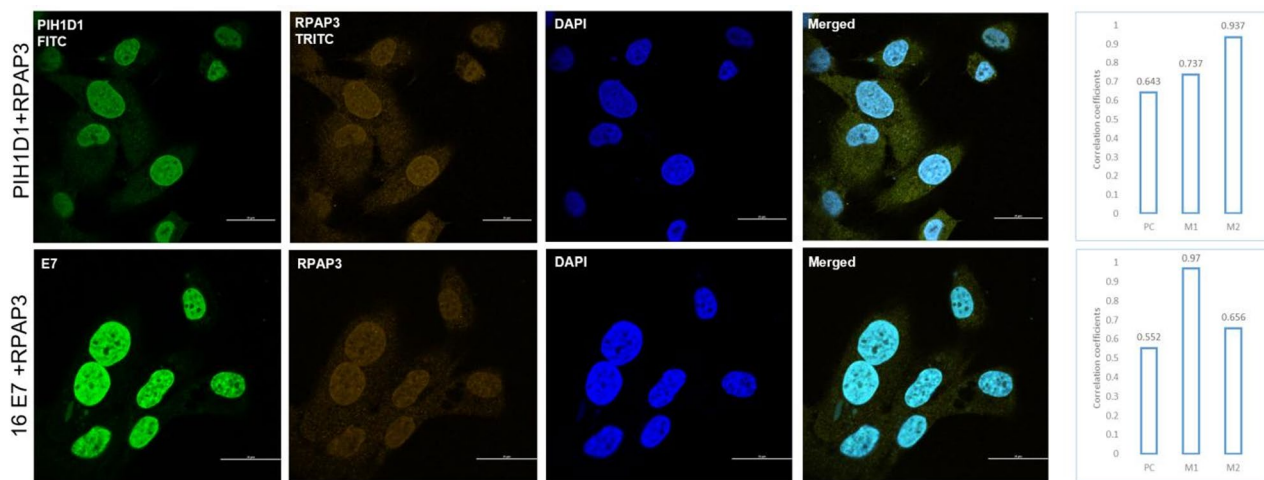


**Fig. 3** Colocalization of HPV16 E7 protein with the R2TP complex. Immunofluorescence analysis of PIH1D1, RPAP3 and E7 in CaSki cells fixed with 4% paraformaldehyde: PIH1D1 and 16E7 (FITC, green), RPAP3 (TRITC, orange), nuclei (DAPI) and merged images. The scale bar is 25  $\mu$ m. Data was analysed with ImageJ software (JACoP) and is representative of three independent experiments. Confocal microscopy images showed PIH1D1 and RPAP3 colocalised to the nucleus and cytoplasm, and E7 and RPAP3 were colocalised to the nucleus. Manders' coefficients (M1 and M2) and Pearson correlation coefficient (PC) values of 1 reflect a complete co-localisation between both images

both serine residues S31/32 were mutated to alanine A31/32. Mutation of both residues completely abolished CK2 phosphorylation of E7, confirming that both these serine residues of E7 are important for PIH1D1 binding.

To further validate the interaction of PIH1D1 and phosphorylated HPV E7 in cells, we subcloned the wild-type and mutant E7 constructs into the eukaryotic expression vector pcDNA3.1+. HEK293 cells were transiently transfected with these wild-type and mutant E7 constructs, and the expression was verified by Western blot. (Fig. 5C). In the same lysates, PIH1D1 was immunoprecipitated, and the blots were probed for 16 E7. As shown in Fig. 5C, PIH1D1 was able to co-immunoprecipitate HPV16 E7 WT and E7 S31A, whereas no interaction was observed between PIH1D1 and either the S32A E7 or S31/32A E7 mutant proteins. The appearance of two E7 bands likely reflects the phosphorylated or unphosphorylated forms of E7, consistent with previous reports describing phosphorylation-induced mobility shifts [33].

#### **E7, R2TP complex and pRB form a complex in cells, and E7 is important for pRB interaction with the R2TP complex in cervical cancer cells**

In Fig. 1, we established the interaction between PIH1D1 and high-risk HPV E7 proteins. The interaction of E7 with pRB was a positive control for the experiments. (Figure 2B and C) Therefore, we investigated whether PIH1D1, E7 and pRB form a complex in cervical cancer cells. To answer this question, we performed an in vitro binding assay by incubating purified GST-PIH1D1 (Fig. 6A) with lysates from MG132-treated CaSki cells. GST-PIH1D1 successfully pulled down both pRB and E7 (Fig. 6B), with the interaction between PIH1D1 and

RPAP3 included as a positive control. (Note: RB and pRB refer to the same retinoblastoma protein; the anti-RB antibody detects hypo- and hyper-phosphorylated forms, therefore, the notation *pRB* is used throughout the text to denote the phosphoprotein. In western blot analysis, RB migrates as multiple closely-spaced bands between 110 and 116 kDa on SDS-PAGE.)

To analyse the role of E7 in mediating the interaction between pRB and PIH1D1, we knock down E7 in CaSki cells using small interfering RNA (100nM siRNA) (Fig. 6C) and then, with the cell lysates, we performed co-immunoprecipitation with an anti-PIH1D1 antibody. (Fig. 6D) Interestingly, depletion of E7 resulted in a reduced amount of pRB co-immunoprecipitated with PIH1D1 (Fig. 6D), hinting that E7 mediate the interaction between pRB and PIH1D1 in cervical cancer cells. We also examined the interaction of the R2TP complex with pRB in HPV-negative cells. PIH1D1 was able to co-immunoprecipitate pRB from T98G cell lysates, which contain a wild-type pRB gene. (Fig. 6E) The interaction with TELO2 serves as the positive control. Additionally, co-immunoprecipitation with an anti-RUVBL1 antibody from the R2TP complex successfully pulled down pRB from T98G cell lysates, along with RPAP3. (Fig. 6F) To confirm these findings, we transfected HEK293 cells with a pRB construct and verified pRB expression by Western blot. (Fig. 6G) The lysate was then incubated with GST-PIH1D1, followed by western blotting with anti-RB antibody. As expected, PIH1D1 successfully interacted with the exogenously expressed pRB. (Fig. 6G)

We confirmed the interaction of PIH1D1 with pRB in HPV-positive SiHa and CaSki cells, as well as in HPV-negative C33A cells, using proximity ligation

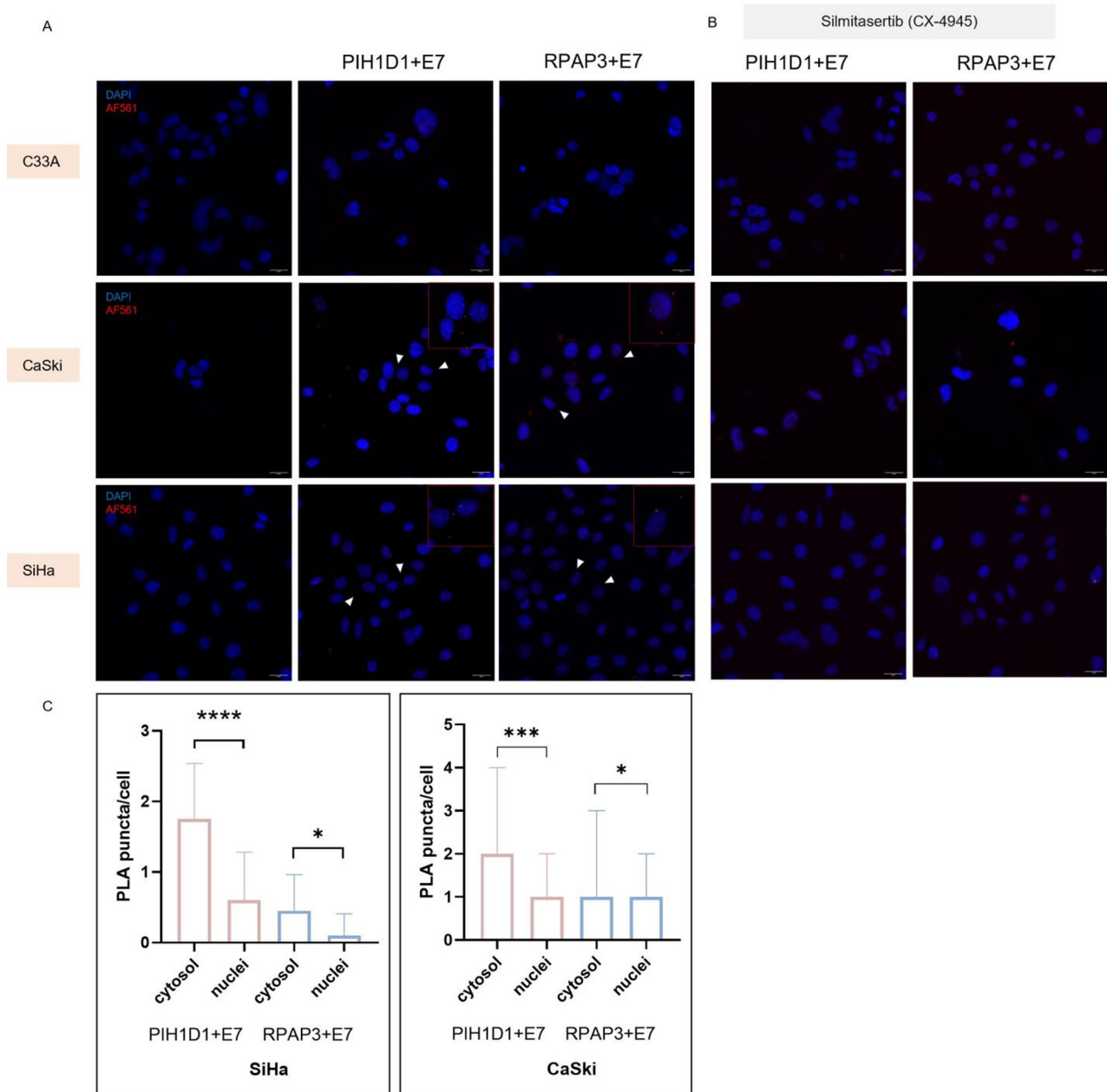


**Fig. 4** Proximity Ligation Assay to visualise the endogenous protein-protein interactions. **A.** C33A, SiHa and CaSki cells were fixed with 4% paraformaldehyde and incubated with antibodies PIH1D1, RPAP3 and 16E7. Data were analysed using Fiji software and are representative of three independent experiments. Cells without the primary antibodies and HPV-negative C33A cells were used as negative controls. Nuclei were stained with DAPI in blue. Each positive interaction is seen as an orange discrete spot. Scale bar: 20  $\mu$ m. Insets show zoomed regions. **B.** C33A, SiHa and CaSki cells were treated with CX-4945 2.5  $\mu$ M for 24 h. Scale bar: 20  $\mu$ m. **C.** Quantification of PLA signals (orange puncta) in the cytosol and nuclei of SiHa and CaSki cells, respectively. Bars indicate median.  $n=20$ , \*\*\*\* $p < 0.0001$ , \*\*\* $p < 0.001$ , \* $p < 0.05$

assay. (Fig. 7) The interaction of PIH1D1 with pRB was observed in the nucleus and cytoplasm. As shown in Fig. 6D, the interaction of pRB with PIH1D1 is weaker in the absence of E7. We postulate that this could explain the reduced interaction observed in HPV-negative cells (T98G, HEK293, C33A), consistent with the fewer PLA puncta seen in C33A cells compared to HPV-positive cells (Fig. 7).

#### PIH1D1 is required for cervical cancer cell proliferation and E7 stability

The precise functions of PIH1D1 within the cell remain unclear. We used a pool of siRNA to deplete PIH1D1 and study the functional consequences. In the MTT assay, depletion of PIH1D1 resulted in a significant decrease in the proliferation of CaSki cells from day 1, i.e. 48 h (24 h post-transfection) to 5, compared to

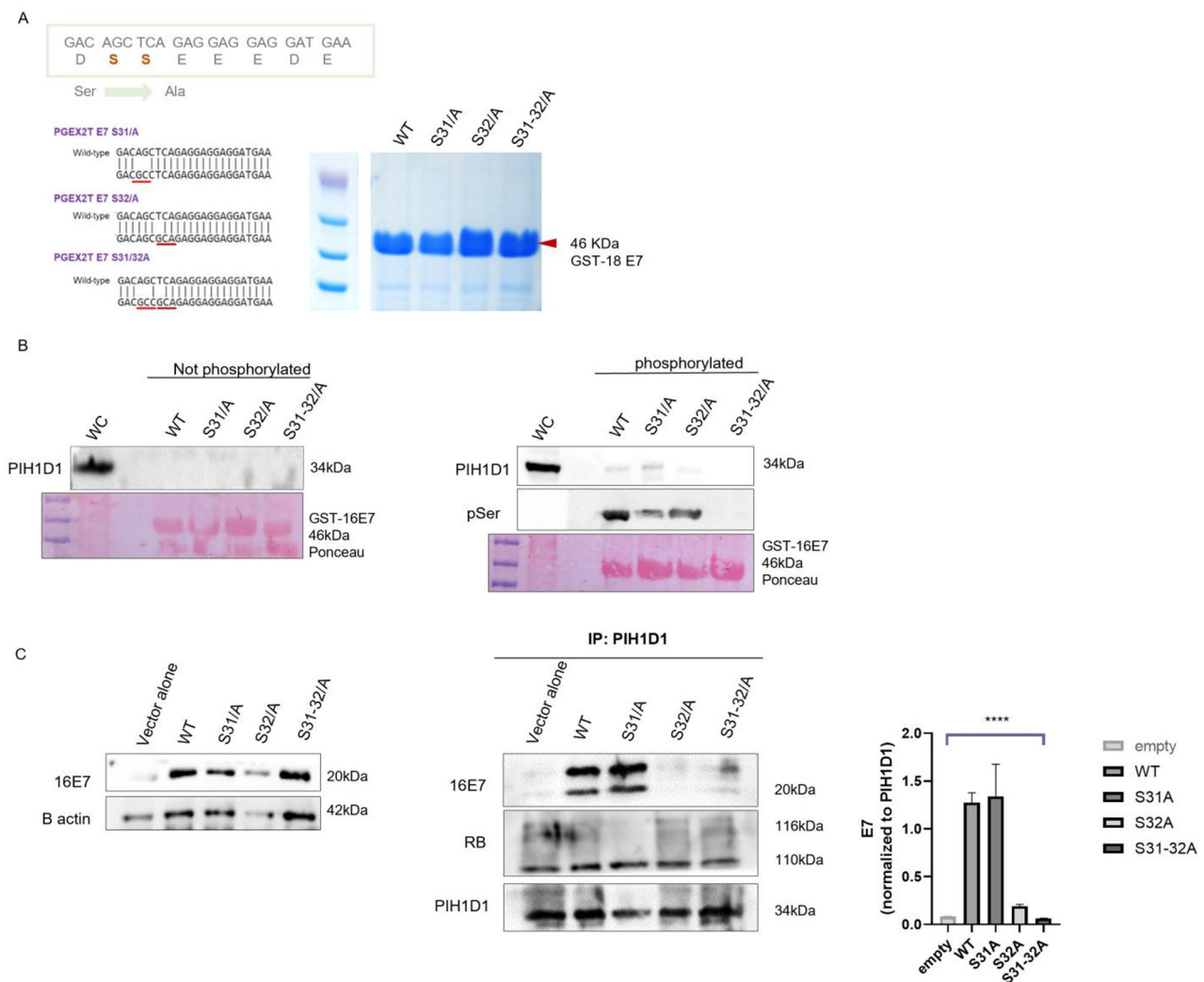


**Fig. 5** The CK2 phosphorylation site of E7 is indispensable for interaction with PIH1D1. **(A)** CK2 motif showing serine residues in HPV16 E7. Serines S31 and S32 were mutated to alanine through site-directed mutagenesis, and the mutations were confirmed by Sanger sequencing. Recombinant GST-tagged E7 proteins were expressed in the *E. coli* BL21 strain, and Coomassie staining shows the purified GST-tagged HPV16 E7 proteins (WT, S31A, S32A, S31/32A). **(B)** HEK293 cell lysates (1 mg) were incubated with GST-tagged, unphosphorylated wild-type and mutant E7 proteins, followed by western blot analysis with an anti-PIH1D1 antibody. HEK293 cell lysates (1 mg) were also incubated with GST-tagged, phosphorylated wild-type and mutant E7 proteins, followed by western blot analysis with anti-PIH1D1 and anti-phosphoserine antibodies. WC represents whole cell lysate. The bottom panel shows the ponceau-stained membrane, indicating total levels of respective GST-E7 proteins (WT, S31A, S32A, S31/32A). **(C)** The pCDNA3.1 + E7(WT, S31, S32, DM) constructs were transfected into HEK293 cells. 48 h post-transfection, cells were lysed in 1% CHAPS buffer supplemented with protease and phosphatase inhibitors. Western Blotting verified the expression of E7 with  $\beta$ -Actin as the loading control. For the interaction analysis, 1  $\mu$ g of anti-PIH1D1 antibody was incubated for 4 h at 4  $^{\circ}$ C with 1 mg of HEK293 cell lysates, respectively, to co-immunoprecipitate the PIH1D1-E7 complex. Control is HEK293 cells transfected with pCDNA3.1+ (empty vector). E7 levels were normalized to PIH1D1 and data is expressed as mean  $\pm$  S (D) ( $n=3$ , \*\*\*\* $p < 0.0001$ )

siScramble-transfected cells. (Fig. 8A) We also performed a wound-healing assay. There was a significant decrease in wound healing in the PIH1D1-depleted CaSki cells, i.e. siPIH1D1 cells migrated more slowly to close the gap of a scratch in the cell monolayer as compared to siScramble cells. (\*\* $p < 0.01$ ) (Fig. 8B) Thus, the depletion of PIH1D1 significantly reduced the cell migration of CaSki cells. Surprisingly, in siPIH1D1 cells, we observed decreased levels of E7. (Fig. 8C) Keeping in view the role of the R2TP complex in stabilising various proteins in the cell,

we performed a half-life assay for the E7 protein in siPIH1D1 and siScramble-transfected HeLa cells. After 72 h of transfection, cells were treated with cycloheximide to block further protein synthesis. The cells were then harvested at 0, 15, 30, 45, 60, and 90 min posttreatment, followed by Western blot analysis of HPV 18 E7 (Fig. 8D). As previously reported [34, 35], the half-life of HPV 18 E7 in cells treated with siScramble lies between 45 and 90 min. However, in the cells treated with siPIH1D1, the half-life of HPV-18 E7 is reduced by half and lies between

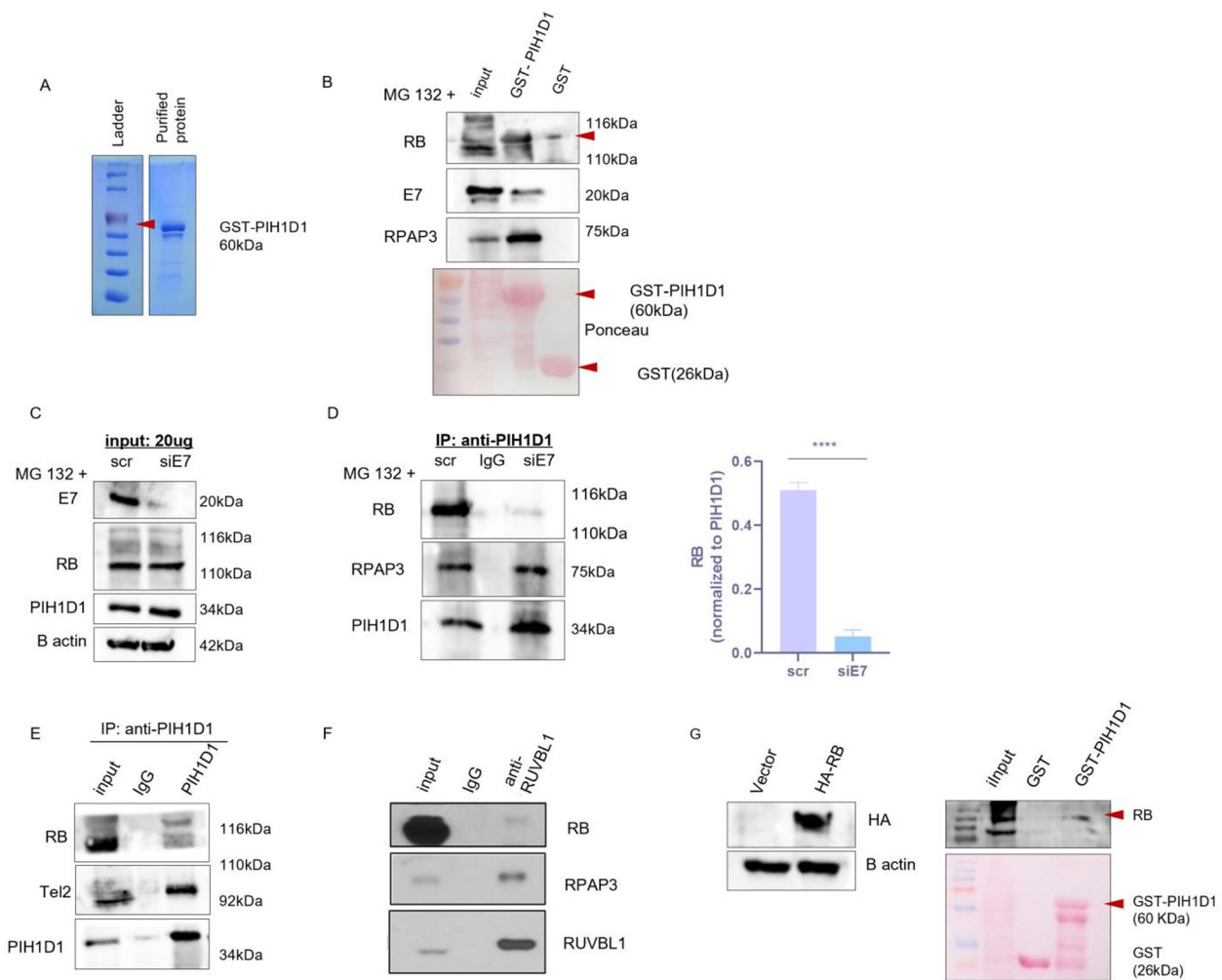


**Fig. 6** The E7 protein, R2TP complex, and pRB form a complex in cells, with E7 facilitating the interaction between pRB and the R2TP complex in cervical cancer cells. **A.** Coomassie staining shows the purified GST-tagged PIH1D1 (~60 kDa) and molecular weight markers (left). PIH1D1 is labile and prone to degradation, as observed in Coomassie staining. **B.** CaSki cells were treated with MG132 to prevent E7-mediated degradation of pRB. CaSki cell lysates (1 mg) were incubated with GST alone and GST-PIH1D1 for four hours, followed by western blotting with anti-pRB, anti-E7, and anti-RPAP3 antibodies. The bottom panel shows the Ponceau-stained membrane, indicating the total levels of GST and GST-PIH1D1 proteins. **C.** CaSki cells were transfected with 100nM siRNA against 16E7. 48 h post-transfection, HPV 16E7, pRB, RPAP3, and PIH1D1 were analysed by western blotting, with  $\beta$ -actin as a control. **D.** CaSki cell lysates treated with scramble or siRNA targeting E7 were subjected to co-immunoprecipitation using 1  $\mu$ g of anti-PIH1D1 antibody, followed by western blotting with antibodies against RB, RPAP3, and PIH1D1. The input represents 20% of the total protein used in the pull-down. pRB levels were normalized to PIH1D1 and data is expressed as mean  $\pm$  S D. ( $n=3$ , \*\*\*\* $p < 0.0001$ ) **E.** 1 mg of T98G cell lysate was subjected to co-immunoprecipitation with anti-PIH1D1 antibody, followed by western blotting with antibodies against pRB, TELO2, and PIH1D1. **F.** 1 mg of T98G cell lysate was subjected to co-immunoprecipitation with anti-RUVBL1 antibody, followed by western blotting with antibodies against pRB, RUVBL1 and RPAP3. **G.** HEK293 cells were transfected with pCMV HA Rb. 48 h post-transfection, the expression was analysed using an anti-HA antibody. Transfected cell lysates were incubated with GST and GST-PIH1D1 proteins, followed by Western Blotting with a pRB antibody. Input was 10% of the total protein used in the pull-down. The bottom panel shows the Ponceau-stained membrane, indicating the total levels of GST and GST-PIH1D1 proteins

30 and 45 min (Fig. 8D). Quantification by densitometric analysis, with each value normalised to B-actin, confirmed a statistically significant reduction in E7 stability. ( $^{**}p < 0.01$ ) These results suggest that PIH1D1 has a stabilising effect on E7 protein levels.

#### Immunohistochemical analysis reveals overexpression of the R2TP complex in cervical cancer

Out of five cervical cancer cases reported in India, four are attributed to infections with HPV types 16 and 18 [36, 37]. We analysed 34 cases of uterine cervical carcinomas diagnosed between November 2023 and January 2024 by the Department of Pathology in AIIMS, Delhi, as well as 10 cases of normal cervical tissue as controls.

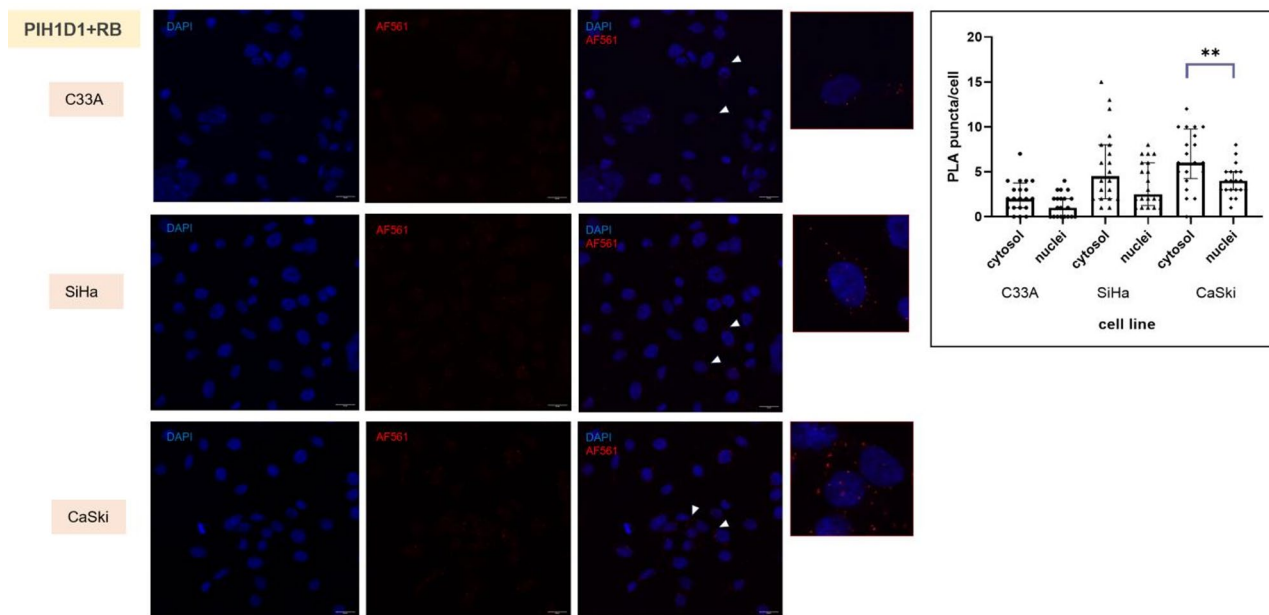


**Fig. 7** Proximity ligation assay for detecting the interaction between PIH1D1 and RB. C33A, SiHa and CaSki cells were fixed with 4% paraformaldehyde and incubated with antibodies PIH1D1 and RB. Data were analysed using Fiji software and are representative of three independent experiments. Cells without the primary antibodies were used as negative controls. Nuclei were stained with DAPI in blue. Each positive interaction is seen as an orange discrete spot. Scale bar: 20  $\mu$ m. Insets on the right show zoomed regions. Quantification of PLA signals (orange puncta) in the cytosol and nuclei of C33A ( $p=0.0596$ ), SiHa ( $p=0.0561$ ) and CaSki (\*\* $p<0.01$ ) cells, respectively. Dots indicate the number of puncta per cell. Bars indicate median.  $n=20$

Patient ages ranged from 30 to 80 years, with a median age of 52 years. Immunohistochemical analysis revealed an overexpression of PIH1D1, RPAP3, and RUVBL1 in cervical cancer tissues compared to normal cervical epithelium. (Fig. 9) PIH1D1 and RPAP3 staining intensities co-varied strongly, while RUVBL1 did not correlate with either. (Table 2) These findings suggest a distinct expression pattern for components of the R2TP complex in cervical cancers, also supporting their potential involvement in HPV-driven oncogenesis.

## Discussion

Our study contributes to an understanding of how HPV proteins, particularly E7 from high-risk HPV types 16 and 18, exploit host cellular proteins to maintain viral persistence and drive oncogenesis in the cervix. Previous research has highlighted the role of CK2-dependent substrate recognition by the R2TP complex, a multiprotein structure comprising the PIH1D1-RPAP3 heterodimer [16, 21, 22]. These subunits play distinct roles in complex assembly and chaperone recruitment; PIH1D1 aids in substrate recognition, while RPAP3 recruits the molecular chaperones Hsp90 and Hsp70 [38, 39]. Our findings establish PIH1D1 as a core subunit that interacts with HPV E7 in both cell-based and in vitro systems. This suggests that this interaction could be a crucial mechanism HPVs employ to support efficient oncogenic processes. (Fig. 10)

Notably, our study revealed that the interaction between PIH1D1 and HPV E7 is phosphorylation-dependent. Mutational analysis of the serine residues within the casein kinase 2 phospho-acceptor site of E7 disrupted this interaction, demonstrating that E7's association with PIH1D1—and, by extension, the R2TP complex—relies on CK2-mediated phosphorylation. This finding establishes E7 as a CK2-dependent client, paralleling other CK2-stabilized proteins that utilize the R2TP complex for their stability and biogenesis [40, 41]. Interestingly, the phosphorylation at serine residue S32 is essential for the interaction with PIH1D1 because PIH1D1 immunoprecipitated HPV16 E7 WT and S31A mutant but not with S32A or the S31-32 A. We cannot exclude the possibility that subtle affinity differences exist between single- and double-phosphorylated E7, as E7 WT and S31A pulled down by PIH1D1 appear comparable in our co-IP assay (ns,  $p$  value = 0.9864). Therefore, while both serine residues can be phosphorylated, our data suggest that the phosphorylation of even a single serine residue (S32) in HPV16 E7 can support the binding with PIH1D1. This observation indicates that HPV types possessing only one serine residue within the CK2 motif may rely on a similar phosphorylation-dependent mechanism, albeit with potentially different binding efficiencies. In the CK2 phospho-acceptor site of HPV18 E7, S34 seems to be the preferred CK2 recognition site, although the S32A mutation appears to enhance the phosphorylation at S34 [27].

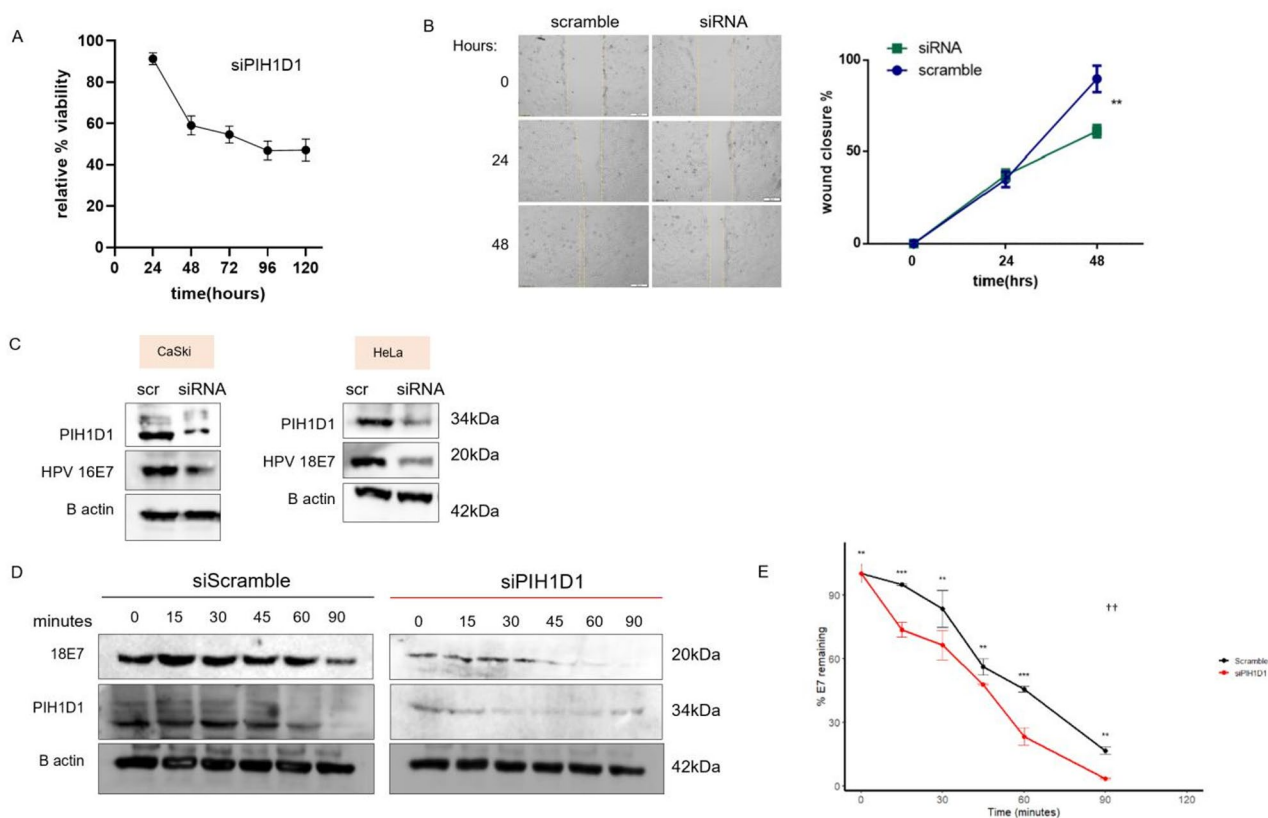


**Fig. 8** PIH1D1 is required for cervical cancer cell proliferation and E7 stability. **(A)** Cell proliferation was measured using an MTT assay. CaSki cells ( $1 \times 10^4$  cells/well) were cultured in a 96-well plate at 37 °C. The following day, the cells were transfected with siRNA against PIH1D1 (100 nM). 100 nM siPIH1D1 was the least toxic concentration that achieved maximal knockdown. MTT was added, and lysates were collected at different time points. The absorbance was measured at 590 nm at the designated time points (24, 48, 72, 96 & 120 h). The y-axis represents relative % viability w.r.t siScramble at each time point. Data is expressed as mean  $\pm$  S D ( $n = 3$ ). **(B)** Wound-healing assays were performed at 0, 24 and 48 h in siPIH1D1 and siScramble CaSki cells. Representative phase-contrast microscope images showing the area covered by the cells at 0, 24 and 48 h after wounding. Original magnification 10  $\times$ . Cell migration was determined by % wound closure, i.e. the rate of cells moving towards the scratched area over time, using ImageJ™ software. Data is expressed as the mean  $\pm$  S D ( $n = 3$ ). (\*\* $p < 0.01$ , scale bar = 200  $\mu$ m). A representative image of three independent experiments is shown. **(C)** PIH1D1 silencing leads to decreased levels of E7 in CaSki and HeLa cells, respectively. Cell lysates from siRNA-transfected cells were collected at 48 h post-transfection. The expression of PIH1D1, HPV16 E7, and HPV18 E7 was analysed by Western blotting. B-actin is a loading control. Scr is scramble siRNA (100nM). **(D)** PIH1D1 modulates E7 protein stability in HeLa cells. Expression of PIH1D1 was silenced using siRNA against PIH1D1, and siScramble was used as the control. After 72 h, cells were treated with cycloheximide. At the indicated time points, lysates were prepared, and Western blotting analysis was performed with antibodies specific for the indicated proteins (right panel); B-actin was used as the loading control. **(E)** Graph indicates the half-life of HPV-18 E7 in the absence and presence of PIH1D1. E7 levels were quantified by densitometry, normalised to B-actin, and plotted as % E7 remaining at 0, 15, 30, 45, 60, and 90 min post-cyclohexamide treatment. For the statistical analysis, a paired t-test was performed for the normalised E7 values between siScramble and siPIH1D1-treated datasets ( $^{**}p < 0.01$ ), and the values at each time point were evaluated using Student's t-test; error bars represent the standard deviation

An intact CK2 phospho-acceptor site in E7 was important for the cell proliferation of cervical cancer-derived C4-1 cells and for maintaining high levels of invasive potential [27]. Notably, although sequence alignment shows variability in the number of serine residues within the CK2 phospho-acceptor site of other high-risk HPV types (Fig. 1C), previous reports indicate that these residues may also be phosphorylated [24, 25]. Thus, single or double phosphorylation across HPV types may differentially influence their interaction with the R2TP complex.

Our results align with existing literature showing the critical role of CK2 in maintaining the stability of HPV E7 to disrupt tumour suppressor pathways, such as pRB.

This establishes CK2 as a promising therapeutic target in HPV-driven malignancies [42, 43]. CK2 inhibitors, including CX-4945 and CIGB-300, have demonstrated efficacy in reducing E7 stability, particularly by diminishing its binding with pRB and disrupting the cell cycle [44, 45]. The drugs augmented the efficacy of cisplatin chemotherapy and improved patient responses, notably in HPV-positive and HPV-negative head and neck squamous cell carcinomas [46]. In our study, treatment of HPV-positive SiHa and CaSki cells with CX-4945 disrupted the interaction between PIH1D1 and E7, thus substantiating that this interaction is CK2 phosphorylation-dependent.

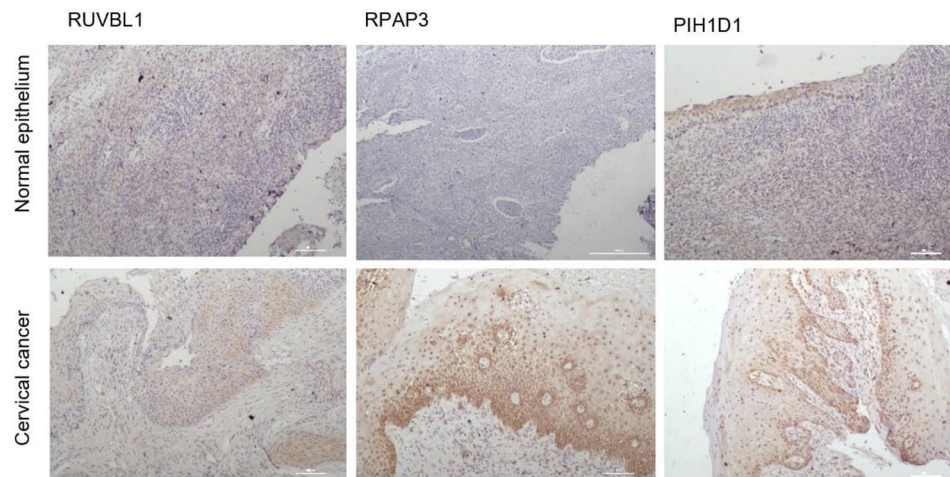


**Fig. 9** RPAP3 and PIH1D1 are overexpressed in cervical cancer patients. Representative images of immunohistochemical expression of RUVBL1, RPAP3 and PIH1D1 in normal epithelium and squamous cell carcinoma of the cervix, respectively. (Scale bar = 100  $\mu$ m for  $\times$ 100magnification) A table showing the Pearson correlation coefficients among the three proteins is presented

**Table 2** Pearson correlation coefficients among proteins RUVBL1, PIH1D1 and RPAP3 in cervical cancer

Pair	Pearson correlation coefficient	p-value
RUVBL1-PIH1D1	0.007	0.969
RUVBL1-RPAP3	0.051	0.774
PIH1D1-RPAP3	0.731	<0.0001

Further supporting the involvement of R2TP in E7-driven oncogenesis, we observed that PIH1D1 binds to pRB *in vitro* and in cellular systems. We found that the interaction between PIH1D1 and pRB decreased when E7 was depleted in cervical cancer cells, CaSki. Therefore, in cervical cancer cells, E7 appears to function as a mediator, facilitating the recruitment of PIH1D1 to pRB to form a complex that likely interferes with pRB's regulation of the E2F1 pathway. This recruitment may represent a strategic mechanism by which HPV undermines cell cycle control, creating conditions conducive to viral replication and persistence in HPV-positive cancers. Interestingly, this binding occurred in both HPV-positive and HPV-negative cells, suggesting that PIH1D1 can independently interact with pRB, potentially via other bridging proteins. This warrants further investigation to determine whether the PIH1D1–pRB interaction is mediated through specific RB isoforms and accessory proteins, particularly in HPV-negative cells. ECD (Ecdysoneless), a CK2 substrate that promotes cell cycle progression, interacts with RUVBL1 and PIH1D1 [47]. ECD competes with E2F for binding to the pocket domain of RB, suggesting a possible role as a bridging factor or competitor in HPV-negative cells. Adding further complexity, ECD selectively binds to high-risk, but not low-risk, HPV E6 proteins and plays a critical role in both viral and host RNA splicing [48].

Beyond the HPV context, the R2TP complex, along with Hsp90, has been implicated in the stabilisation of multiple oncoproteins, and our findings highlight its importance in cervical cancer. Depleting PIH1D1 in HPV-positive cell lines, such as CaSki and HeLa, resulted in the destabilization of E7 and impaired cell proliferation and migration. Notably, we did not observe any significant alterations in the cell cycle distribution, indicating that the depletion of PIH1D1 did not result in any phase-specific cell cycle arrest. Given the established roles of PIH1D1 in ribosome biogenesis, transcription, and post-translational regulation [49], the effects observed are likely indirect and reflect a reduction in overall proliferative capacity rather than impaired cell cycle progression *per se*. Consistent with this interpretation, knockdown of PIH1D1 also led to such stalling in HPV-negative cell lines such as MCF7 and T98G, stating its broader role as an essential component of the R2TP co-chaperone. (Suppl. Figures 2,3) These findings highlight the role of PIH1D1 in maintaining the proliferative capacity across diverse cellular contexts. However, in cervical cancer cells, HPV appears to hijack the chaperone machinery—particularly via E7-mediated recruitment of PIH1D1 to pRB—thus subverting the normal cell cycle control. Further validation in patient-derived samples and *in vivo* models will be required to establish the clinical relevance of this mechanism in HPV-associated malignancies.

In HPV-driven malignancies, E7 proteins serve as pivotal drivers of oncogenesis, with knockouts of HPV18 E6/E7 in HeLa cells resulting in decreased E7 expression, activation of p53 and pRB pathways, and subsequent cellular senescence [7]. pRB, while a degradation target of HPV E7, is also essential for E7 stabilisation. Its continued expression supports the stability and oncogenic function of HPV 16/18 E7, as pRB knockdown destabilises

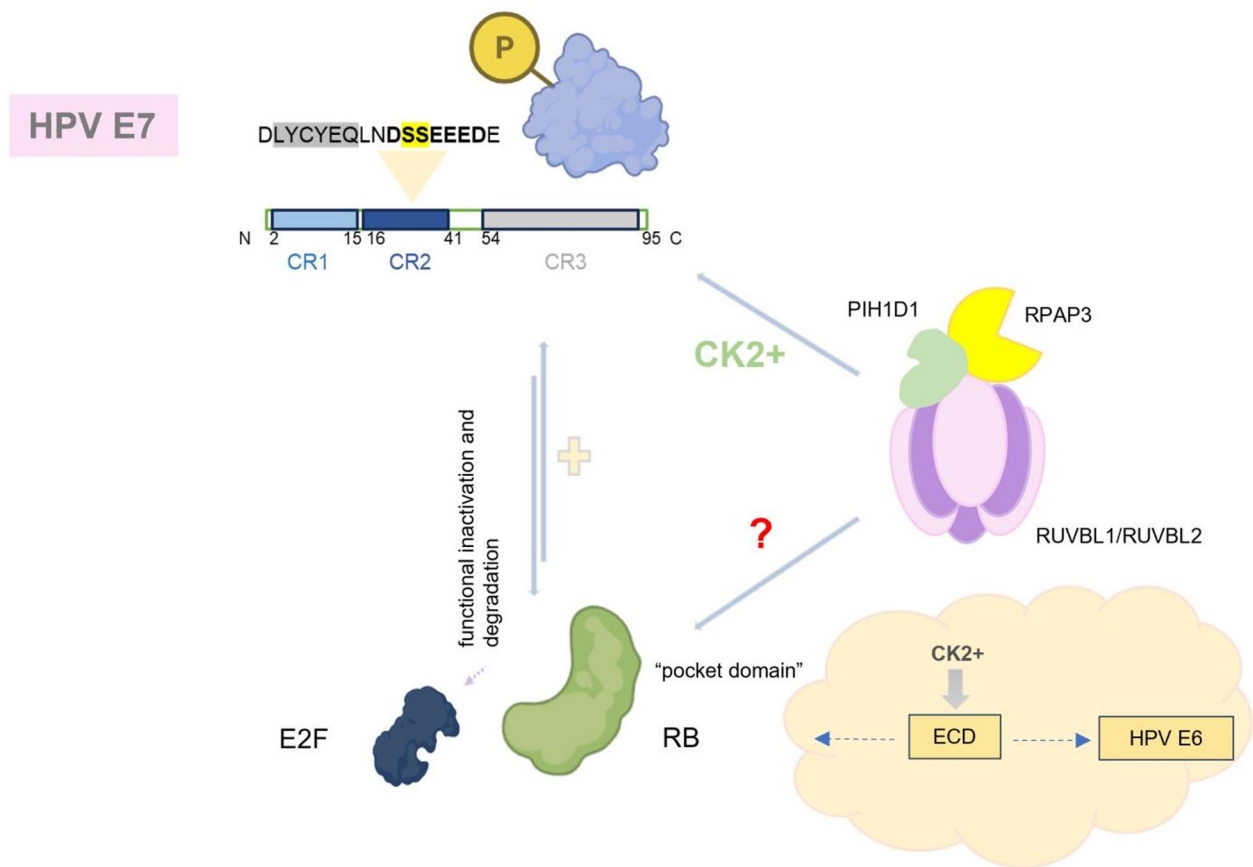


**Fig. 10** HPV E7 and E6 converge on PIH1D1 and ECD to recruit the R2TP complex to pRB. In HPV-infected cervical cancer cells, the viral oncoprotein E7 binds to the tumour suppressor pRB via its conserved LXCXE motif, thereby displacing E2F1 to drive cell cycle progression. Our study established that PIH1D1, a core subunit of the R2TP complex, interacts with E7 in a casein kinase 2 (CK2)-dependent manner. E7 recruits the R2TP complex to the pRB–E7 complex, a mechanism likely facilitating E7 stabilisation and promoting proliferation and migration. In HPV-negative cells, PIH1D1 also interacts with pRB, potentially through CK2-phosphorylated Ecdysoneless (ECD), a cell cycle regulator that binds the pocket domain of pRB in a competition with E2F. Thus, ECD acts as a scaffold linking pRB to the R2TP complex. ECD also binds high-risk HPV E6 oncoproteins. (Created with BioRender.com.)

E7 and inhibits colony formation in SiHa and HeLa cells [35]. Our data shows the R2TP stabilises HPV E7 to drive cellular proliferation. This aligns with the concept of “oncogene addiction,” where cervical cancer cells might rely on R2TP-mediated stabilisation of E7 for sustained growth and survival. This conclusion raises intriguing questions about the dynamics of their interaction. Why does the small E7 protein require a large heteromultimeric complex for its stability?

In addition to affecting cancer cells, RUVBL1, PIH1D1 and RPAP3 interact with the polymerase L proteins of mumps virus (MuV) and measles virus (MeV) [50]. Silencing of the R2TP complex enhanced paramyxoviral RNA synthesis by enhancing the expression of viral transcripts and proteins. However, MuV L1 did not coimmunoprecipitate with the N-terminal domain of PIH1D1, suggesting that the interaction between the MuV L protein and PIH1D1 was mediated through another recognition mechanism. Thus, other CK2-independent clients are recruited by PIH1D1/R2TP.<sup>50</sup> The nucleoproteins of

the Ebola virus also colocalised with RPAP3 and PIH1D1. siRNA-mediated knockdown of RPAP3 and subsequent downregulation of PIH1D1 suggest that RPAP3 plays a role in capsid assembly [51]. These interactions raise intriguing possibilities of the R2TP complex as a host factor in viral pathogenesis.

Additional data support the role of R2TP in cellular proliferation. In mice, PIH1D1 and RPAP3 were expressed in proliferating intestinal stem cells, with RPAP3 loss leading to p53 stabilisation and cell cycle arrest in these cells [17]. The complex is highly expressed in other cancers, including colorectal and oral cancers, where its expression correlates with aggressive tumour phenotypes [17, 18, 20]. Our study mirrors findings in other malignancies.<sup>18,20</sup> Tumour tissues exhibit cellular heterogeneity, with subsets of quiescent or dividing cells. Such conditions may induce dynamic shuttling of R2TP complex proteins between nuclear and cytoplasmic compartments. Consistent with previous reports in cell lines [52, 53], PIH1D1-RPAP3 and HPV E7 were

localised in both the nucleus and cytoplasm. HPV16 E7 also shuttles between the nucleus and cytoplasm [54, 55]. The interactions of PIH1D1 with E7 and pRB were observed to be predominantly cytoplasmic rather than nuclear. The subcellular distribution of R2TP complex proteins was shown to be dynamically regulated by cellular proliferation, growth phase, and nutrient conditions, with predominant nuclear localisation observed during proliferative phases through a Kap121-dependent mechanism, facilitating box C/D snoRNP assembly and ribosome biogenesis. In contrast, R2TP proteins actively shuttle to the cytoplasm via a Crm1-dependent pathway under nutrient-limiting or stationary conditions, impairing ribosome biogenesis [56]. Therefore, our findings, combined with these earlier observations, strongly warrant further investigation into how proliferation states can influence the localisation and functions of the R2TP complex components.

Overall, our study calls for investigations into the list of R2TP and R2TP/PFDL clients involved in protein synthesis, cell growth and metabolism, gene expression and genome stability. We believe that additional clients remain to be identified. While interactions might be direct or indirect, we have yet to distinguish between CK2-dependent and independent interactions and their cellular consequences..

### Supplementary Information

The online version contains supplementary material available at <https://doi.org/10.1186/s12985-026-03070-z>.

Supplementary Material 1.

### Acknowledgements

We thank the authors and collaborators for their valuable contributions to this project. We thank Dr Saumitra Dey Choudhury, Confocal Microscopy Facility, Centralised Core Research Facility, AIIMS, New Delhi, for his kind assistance in acquiring the confocal microscopy images. We thank Dr K David Raja for reviewing the manuscript and for the valuable assistance with data visualisation.

### Author contributions

Mahaiwon Shadang: Investigation, Writing - Original Draft, Writing - Review & Editing, Formal analysis, Visualisation. Aruna Arumugam: Investigation, Writing - Review & Editing. Dhiraj Kumar Singh: Investigation (Supplementary Figure 3). Pankaj Keshari: Validation (Figure 6G). Sandeep Mathur: Resources, Validation. Venkateswaran K. Iyer: Resources. Seema Singhal: Resources. Shyam S Chauhan: Resources. Qulsum Akhter: Review. Riyaz Ahmad Mir: Conceptualisation, Supervision, Funding acquisition, Review & Editing.

### Funding

This work was supported by research grants SERB No: 9330/2018–2019, from the Science and Engineering Research Board, Department of Science and Technology, Government of India and Project ID: IIRPSG-2024-01-03511 from the Indian Council of Medical Research, India. Mahaiwon Shadang was a recipient of the Senior Research Fellowship, Council of Scientific & Industrial Research (CSIR), India.

### Data availability

All the data generated have been incorporated into the manuscript or provided as supplementary material. Further inquiries can be directed to the corresponding author.

### Declarations

#### Ethics approval and consent to participate

Ethical clearance was obtained from the institutional review board, All India Institute of Medical Sciences (AIIMS), New Delhi, India. (IECPG-152/23.04.2020) The formalin-fixed, paraffin-embedded tissue blocks were obtained from the archives of the Department of Pathology, AIIMS, New Delhi, India.

#### Consent for publication

All authors have approved the manuscript for submission and publication.

#### Competing interests

The authors declare no competing interests.

Received: 14 August 2025 / Accepted: 5 January 2026

Published online: 05 March 2026

### References

1. de Martel C, Georges D, Bray F, Ferlay J, Clifford GM. Global burden of cancer attributable to infections in 2018: a worldwide incidence analysis. *Lancet Glob Health*. 2020;8:e180–90.
2. Bray F, et al. Global cancer statistics 2022: GLOBOCAN estimates of incidence and mortality worldwide for 36 cancers in 185 countries. *CA Cancer J Clin*. 2024;74:229–63.
3. Pf C, S, B, L, L, Rj K. Biology of HPV mediated carcinogenesis and tumor progression. *Semin Radiat Oncol* 2021;31(4):265–273.
4. Wei F, Georges D, Man I, Baussano I, Clifford GM. Causal attribution of human papillomavirus genotypes to invasive cervical cancer worldwide: a systematic analysis of the global literature. *Lancet Lond Engl*. 2024;404:435–44.
5. Pal A, Kundu R. Human Papillomavirus E6 and E7: the cervical cancer hallmarks and targets for therapy. *Front Microbiol*. 2019;10:3116.
6. Vats A, Trejo-Cerro O, Thomas M, Banks L. Human papillomavirus E6 and E7: what remains? *Tumour Virus Research*. 2021;11:200213.
7. Inturi R, Jemth P. CRISPR/Cas9-based inactivation of human papillomavirus oncogenes E6 or E7 induces senescence in cervical cancer cells. *Virology*. 2021;562:92–102.
8. Jones DL, Thompson DA, Munger K. Destabilization of the RB tumor suppressor protein and stabilization of p53 contribute to HPV type 16 E7-induced apoptosis. *Virology*. 1997;239:97–107.
9. Scheffner M, Huibregtse JM, Vierstra RD, Howley PM. The HPV-16 E6 and E6-AP complex functions as a ubiquitin-protein ligase in the ubiquitination of p53. *Cell*. 1993;75:495–505.
10. Wise-Draper TM, Wells SI. Papillomavirus E6 and E7 proteins and their cellular targets. *Front Biosci-Landmark*. 2008;13:1003–17.
11. Munger K, Phelps WC, Bubb V, Howley PM, Schlegel R. The E6 and E7 genes of the human papillomavirus type 16 together are necessary and sufficient for transformation of primary human keratinocytes. *J Virol*. 1989;63:4417–21.
12. Boyer SN, Wazer DE, Band V. E7 protein of human papilloma virus-16 induces degradation of retinoblastoma protein through the ubiquitin-proteasome pathway. *Cancer Res*. 1996;56:4620–4.
13. Zhao R, et al. Navigating the chaperone network: an integrative map of physical and genetic interactions mediated by the hsp90 chaperone. *Cell*. 2005;120:715–27.
14. Rivera-Calzada A, et al. The structure of the R2TP complex defines a platform for recruiting diverse client proteins to the HSP90 molecular chaperone system. *Structure*. 2017;25:1145–1152.e4.
15. Houry WA, Bertrand E, Coulombe B. The paqosome, an R2TP-based chaperone for quaternary structure formation. *Trends Biochem Sci*. 2018;43:4–9.
16. Shadang M, Ahmad Mir R. PIH1D1 and RPAP3, components of the paqosome: emerging roles in cellular physiology. *Mol Cell Biol*. 2025;0:1–16.
17. Maurizy C, et al. The HSP90/R2TP assembly chaperone promotes cell proliferation in the intestinal epithelium. *Nat Commun*. 2021;12:4810.

18. Kiguchi T, et al. Identification and characterization of R2TP in the development of oral squamous cell carcinoma. *Biochem Biophys Res Commun*. 2021;548:161–6.
19. Kamano Y, et al. PIH1D1 interacts with mTOR complex 1 and enhances ribosome RNA transcription. *FEBS Lett*. 2013;587:3303–8.
20. Lone M, et al. The expression of the RUVBL1 component of the R2TP complex correlates with poor prognosis in DLBCL. *Pathobiology*. 2022;89:146–56.
21. Hořejší Z, et al. Phosphorylation-dependent PIH1D1 interactions define substrate specificity of the R2TP cochaperone complex. *Cell Rep*. 2014;7:19–26.
22. von Morgen P, Hořejší Z, Macurek L. Substrate recognition and function of the R2TP complex in response to cellular stress. *Front Genet*. 2015;6:69.
23. Negative charge at the casein kinase II phosphorylation site is important for transformation but not for Rb protein binding by the E7 protein of human papillomavirus type 16. *Proc Natl Acad Sci U S A*. 1991;88(12):5187–91. <https://pubmed.ncbi.nlm.nih.gov/2052600/>
24. Basukala O, Sarabia-Vega V, Banks L. Human papillomavirus oncoproteins and post-translational modifications: generating multifunctional hubs for overriding cellular homeostasis. *Biol Chem*. 2020;401:585–99.
25. Trejo-Cerro O, Broniarczyk J, Kavcic N, Myers M, Banks L. Identification and characterisation of novel potential phospho-acceptor sites in HPV-16 E7. *Tumour Virus Research*. 2023;16:200270.
26. Barbosa MS, et al. The region of the HPV E7 oncoprotein homologous to adenovirus E1a and Sv40 large T antigen contains separate domains for Rb binding and casein kinase II phosphorylation. *EMBO J*. 1990;9:153–60.
27. Basukala O, Mittal S, Massimi P, Bestagno M, Banks L. The HPV-18 E7 CKII phospho acceptor site is required for maintaining the transformed phenotype of cervical tumour-derived cells. *PLoS Pathog*. 2019;15:e1007769.
28. Chien WM, Parker JN, Schmidt-Grimminger DC, Broker TR, Chow LT. Casein kinase II phosphorylation of the human papillomavirus-18 E7 protein is critical for promoting S-phase entry. *Cell Growth Differ Mol Biol J Am Assoc Cancer Res*. 2000;11:425–35.
29. Helt A-M, Galloway DA. Mechanisms by which DNA tumor virus oncoproteins target the Rb family of pocket proteins. *Carcinogenesis*. 2003;24:159–69.
30. Seifried LA, et al. pRB-E2F1 complexes are resistant to Adenovirus E1A-mediated disruption. *J Virol*. 2008;82:4511–20.
31. Shin M-K, Sage J, Lambert PF. Inactivating all three Rb family pocket proteins is insufficient to initiate cervical cancer. *Cancer Res*. 2012;72:5418–27.
32. Helt A-M, Galloway DA. Destabilization of the retinoblastoma tumor suppressor by human papillomavirus type 16 E7 is not sufficient to overcome cell cycle arrest in human keratinocytes. *J Virol*. 2001;75:6737–47.
33. Valdovinos-Torres H, et al. Different isoforms of HPV-16 E7 protein are present in cytoplasm and nucleus. *Open Virol J*. 2008;2:15–23.
34. E R, M, S., M, O., A, C., A S. Degradation of the E7 human papillomavirus oncoprotein by the ubiquitin-proteasome system: targeting via ubiquitination of the N-terminal residue. *Oncogene* 2000;19(51):5944–50.
35. Gbala I, Kavcic N, Banks L. The retinoblastoma protein contributes to maintaining the stability of HPV E7 in cervical cancer cells. *J Virol*. 2025;99:e02203–24.
36. Satapathy P, et al. Prevalence of human papilloma virus among cervical cancer patients in India: a systematic review and meta-analysis. *Medicine (Baltimore)*. 2024;103:e38827.
37. Ramamoorthy T, Sathishkumar K, Das P, Sudarshan KL, Mathur P. Epidemiology of human papillomavirus related cancers in India: findings from the National cancer registry programme. <http://ecancer.org/en/journal/article/1444-epidemiology-of-human-papillomavirus-related-cancers-in-india-findings-from-the-national-cancer-registry-programme>. 2022. <https://doi.org/10.3332/ecancer.2022.1444>.
38. Henri J, et al. Deep structural analysis of RPAP3 and PIH1D1, two components of the HSP90 co-chaperone R2TP complex. *Structure*. 2018;26(9):1196–1209.e8.
39. RPAP3 provides a flexible scaffold for coupling HSP90 to the human R2TP co-chaperone complex. *Nature communications*. 2018;9(1):1501. <https://www.nature.com/articles/s41467-018-03942-1>
40. MRE11 stability. Is regulated by CK2-dependent interaction with R2TP complex. *Oncogene* 2017; 36, 4943–4950. <https://www.nature.com/articles/onc201799>
41. Horejsi Z, et al. CK2 phospho-dependent binding of R2TP complex to TEL2 is essential for mTOR and SMG1 stability. *Mol Cell*. 2010;39:839–50.
42. Homma MK, et al. Cell cycle-dependent gene networks for cell proliferation activated by nuclear CK2α complexes. *Life Sci Alliance*. 2023;7:e202302077.
43. Piirsoo A, et al. Activity of CK2α protein kinase is required for efficient replication of some HPV types. *PLoS Pathog*. 2019;15:e1007788.
44. Ramón AC, et al. CIGB-300 peptide targets the CK2 phospho-acceptor domain on human papillomavirus E7 and disrupts the retinoblastoma (RB) complex in cervical cancer cells. *Viruses*. 2022;14:1681.
45. Rabalski AJ, Gyenis L, Litchfield DW. Molecular pathways: emergence of protein kinase CK2 (CSNK2) as a potential target to inhibit survival and DNA damage response and repair pathways in cancer cells. *Clin Cancer Res*. 2016;22:2840–7.
46. Trembley JH, et al. CX-4945 and siRNA-Mediated Knockdown of CK2 Improves Cisplatin Response in HPV(+) and HPV(–) HNSCC Cell Lines. *Bio-medicines*. 2021;9:571.
47. Mir RA, et al. A novel interaction of ecdysoneless (ECD) protein with R2TP complex component RUVBL1 is required for the functional role of ECD in cell cycle progression. *Mol Cell Biol*. 2016;36:886–99.
48. Mirza S, et al. Ecdysoneless protein regulates viral and cellular mRNA splicing to promote cervical oncogenesis. *Mol Cancer Res*. 2022;20:305–18.
49. Lynham J, Houry WA. The role of Hsp90-R2TP in macromolecular complex assembly and stabilization. *Biomolecules*. 2022;12:1045.
50. Katoh H, et al. The r2tp complex regulates paramyxovirus RNA synthesis. *PLoS Pathog*. 2019;15:e1007749.
51. Morwitzer MJ, et al. Identification of RUVBL1 and RUVBL2 as novel cellular interactors of the Ebola virus nucleoprotein. *Viruses*. 2019;11:372.
52. Palacios-Abella A, et al. The structure of the R2T complex reveals a different architecture from the related HSP90 cochaperone R2TP. *Structure*. 2025;33:740–752.e8.
53. Ni L, et al. Rpap3 interacts with reptin to regulate uv-induced phosphorylation of H2ax and dna damage. *J Cell Biochem*. 2009;106:920–8.
54. Dreier K, et al. Subcellular localization of the human papillomavirus 16 E7 oncoprotein in CaSki cells and its detection in cervical adenocarcinoma and adenocarcinoma in situ. *Virology*. 2011;409:54–68.
55. Laurson J, Raj K. Localisation of human papillomavirus 16 E7 oncoprotein changes with cell confluence. *PLoS One*. 2011;6:e21501.
56. Kakiyama Y, Makhnevych T, Zhao L, Tang W, Houry WA. Nutritional status modulates box C/D snoRNP biogenesis by regulated subcellular relocalization of the R2TP complex. *Genome Biol*. 2014;15:404.
57. Radstake WE, et al. Comparison of *in vitro* scratch wound assay experimental procedures. *Biochem Biophys Rep*. 2023;33:101423.

## Publisher's note

Springer Nature remains neutral with regard to jurisdictional claims in published maps and institutional affiliations.